JGR Oceans

RESEARCH ARTICLE
10.1029/2021JC017275

Mixing Efficiency for Breaking Internal Solitary Waves

Giovanni la Forgia[1], Davide Cavaliere[1,2], Claudia Adduce[1,3], and Federico Falcini[1]

[1]Institute of Marine Sciences, National Research Council, Rome, Italy, [2]Department of Basic and Applied Sciences for Engineering, Sapienza University of Rome, Rome, Italy, [3]Department of Engineering, Roma Tre University, Rome, Italy

Key Points:

- Heuristic model to quantify mixing induced by breaking internal solitary waves (ISWs)
- Experimental estimation of the change in the total background potential energy
- Prediction of the mixing efficiency for breaking ISWs

Correspondence to:

D. Cavaliere,
davide.cavaliere@artov.ismar.cnr.it

Citation:

la Forgia, G., Cavaliere, D., Adduce, C., & Falcini, F. (2021). Mixing efficiency for breaking internal solitary waves. *Journal of Geophysical Research: Oceans*, *126*, e2021JC017275. https://doi.org/10.1029/2021JC017275

Received 10 FEB 2021
Accepted 15 APR 2021

Abstract We propose a semi-analytic approach to estimate mixing induced by internal solitary waves (ISWs) breaking over a sloping boundary. The theoretical framework we develop describes the energetics of a stratified fluid flow during the interaction of ISWs with a slope. In particular, through both Ozmidov and Thorpe lengthscales we derive a heuristic expression for mixing efficiency, valid for plunging and plunging-collapsing breakers. On the other hand, we perform laboratory experiments that also provide mixing efficiency by estimating both changes of the background potential energy and the incident and reflected ISWs energy. We then compare those results with the ones derived by our theoretical model, obtaining a power law that relates the two quantities. This function allows to estimate mixing efficiency when the change in the background potential energy due to the ISWs breaking is unknown. We finally successfully apply our model to estimate the mixing efficiency under real field conditions.

Plain Language Summary Internal solitary waves (ISWs), generated by tide-topography interactions or river plumes, represent one of the most energetic phenomena in the coastal oceans. Mixing due to ISWs breaking has a profound impact on water stratification, biological productivity, sediment resuspension and general oceanic energy balance. Through the mixing efficiency parameter, it is possible to give an estimation of the amount of incident wave energy contributing to the irreversible mixing of the density field. In this work, we study the breaking of ISWs over a sloping boundary by laboratory experiments, and we provide a heuristic semi-analytic expression for the variation of the background potential energy, associated to the irreversible mixing process, and thus for the mixing efficiency. We also give an estimation of the mixing efficiency and we examine its relevance in real field environment.

1. Introduction

Internal solitary waves (ISWs, or "internal solitons") consist in large displacements of the pycnocline with a permanent bell-shaped form, resulting from a balance between nonlinear and dispersive effects (Grimshaw, Pelinovsky, Talipova, & Kurkina, 2010; Grue, 2006; Helfrich & Melville, 2006; Massel, 2015; Osborne & Burch, 1980). They propagate in density-stratified fluids in response of gravitational restoring forces, acting on vertically displaced fluid, and they are mostly generated by river plumes (la Forgia, Ottolenghi, et al., 2020; Nash & Moum, 2005; Ottolenghi, Adduce, Roman, & la Forgia, 2020; Pan et al., 2007) and tide-topography interactions (Alpers et al., 2008; Brandt et al., 1999; Jackson et al., 2013).

Theoretically, ISWs propagation is usually described by weakly nonlinear models, as Korteweg–De Vries (KdV) (Osborne & Burch, 1980) and Gardner equations (Grimshaw, Pelinovsky, Talipova, & Kurkin, 2004; Grimshaw, Pelinovsky, Talipova, & Kurkina, 2010), and strongly nonlinear models, as Miyata–Choi–Camassa (MCC) model (Choi & Camassa, 1999; Kodaira et al., 2016; Miyata, 1985) and Dubreil-Jacotin-Long (DJL) equation (Dubreil-Jacotin, 1937; Long, 1953; Stasna & Lamb, 2002).

Breaking and dissipation of internal solitons on continental slopes have significant implications for mixing and sediment transport. Near-bed instabilities and shear stress, associated with strong currents beneath ISWs, trigger sediment resuspension (Boegman & Stasna, 2019; Bogucki et al., 1997). As a consequence, solitons may play an important role in shaping the seafloor, by transporting sediment in both the downslope and upslope directions (Cacchione et al., 2002; Cavaliere et al., 2021; Martorelli et al., 2020; Puig et al., 2004), and generating peculiar sediment patterns (Droghei et al., 2016; La Forgia, Adduce, Falcini, & Paola, 2019).

During ISWs breaking, the occurrence of large-scale instabilities and eddies at the interface enhances turbulence between the two adjacent fluids. This causes the development of diapycnal mixing as the fluid parcels, entrained

into the intermediate layer, are redistributed by chaotic advection and stretched in response to the large strain rates produced by turbulence (Peltier & Caulfield, 2003).

Turbulence due to breaking internal waves accounts for a significant sink of energy at ocean boundaries (Ferrari et al., 2016; McDougall & Ferrari, 2017; Munk & Wunsch, 1998; Wunsch & Ferrari, 2004), and it may represent a key factor in closing the abyssal circulation (Artale et al., 2018; Mashayek et al., 2017). Moreover, the resulting mixing acts modifying the stratification and enhancing biological productivity (Lamb, 2014; Woodson, 2018).

Mixing is usually quantified by the *mixing efficiency*, that is, the amount of kinetic energy irreversibly converted into background potential energy as well as the amount of incident wave energy contributing to irreversible mixing of the density field (Gregg et al., 2018; Osborn, 1980; Winters et al., 1995). Still today, semi-empirical parametrizations assume a constant mixing efficiency for the whole ocean, of about 0.2 (Nikurashin & Ferrari, 2013), although there is clear consensus from laboratory and direct numerical simulations that mixing efficiency is highly variable and changes with mechanism, evolutionary stage of a turbulent event, and location in the domain (Barry et al., 2001; Bouffard & Boegman, 2013; Ivey et al., 2008; Shih et al., 2005; Smyth et al., 2001). In particular, a variety of laboratory and DNS experiments (e.g., Barry et al. [2001] and Shih et al. [2005]; for a complete review, we refer the reader to Ivey et al. [2008] and Gregg et al. [2018]) investigated the variability of mixing efficiency as function of the Reynolds buoyancy number (Re_b), which represents the ratio between turbulent stirring and effects of buoyancy and viscosity. These studies showed a nonlinear dependency of mixing efficiency on Re_b, reaching the maximum value of 0.2 for Re_b of $O(10^2)$. In the ocean, Re_b varies from $O(1)$ (e.g., Wuest & Lorke, 2005) to $O(10^5)$, in deep regions (e.g., Ferron et al. [1998]) and, consequently, the use of a constant value for mixing efficiency is inaccurate. Furthermore, observations show that the oceans are not uniformly and steadily agitated, but there is a relatively quiescent interior and turbulent hot spots, often near boundaries (Artale et al., 2018; Wunsch & Ferrari, 2004). Thus, it is important to determine the geography of mixing hot spots and the dynamics responsible for their spatial and temporal distribution. In particular, mixing is enhanced through the water column in those regions that are characterized by rough bathymetry (Kokoszka et al., 2019; Ledwell et al., 2000; Mashayek et al., 2017; Polzin et al., 1997; St. Laurent et al., 2012). However, seafloor-induced turbulence is expected to occur within the bottom boundary layer. This suggests that internal waves are likely responsible for transport energy up from the bottom, due to their interaction with bathymetric features such as seamounts, sills, ridges and continental slopes (Cavaliere et al., 2021; Polzin et al., 1997).

Field observations estimated energetics of shoaling and breaking internal waves (e.g., Davis & Monismith, 2011; Klymak et al., 2008; Scotti et al., 2006; Shroyer et al., 2010; Walter et al., 2012). However, these results are limited by the spatial and temporal resolution of field data. For this, laboratory and numerical studies have been widely carried out by using small-scale idealized domains. Helfrich (1992) performed laboratory experiments on shoaling and breaking ISWs interacting with a sloping boundary, where the interface intersected the bottom and breaking occurred in all cases. These experiments allowed to measure the mixing efficiency, defined as the ratio between the change in potential energy near the breaking point (i.e., ΔE_p) and the net energy into the breaking region:

$$\epsilon = \frac{\Delta E_p}{E_0 - E_R} = \frac{\Delta E_p}{E_0(1 - R)}, \tag{1}$$

where E_0 is the incident wave energy, E_R is the reflected energy and $R = E_R/E_0$ is the reflectance coefficient. In particular, it was found that diapycnal mixing induced by wave breaking led to a loss of energy, $\epsilon = 0.15 \pm 0.05$, expended in increasing the potential energy of the stratification by raising the water mass center (Helfrich, 1992). Michallet and Ivey (1999) extended the results for larger ISWs, finding that mixing efficiency was related to the ratio L_w/L_s, where L_w is the characteristic horizontal scale of the incident wave and L_s the length scale of the slope; they also found a maximum mixing efficiency value of about 0.25.

ISWs breaking mechanisms can be classified by the *internal Iribarren number*, that is, the ratio of the topographic slope to the square root of the wave slope (Boegman et al., 2005):

$$Ir = \frac{s}{\sqrt{S_w}}, \tag{2}$$

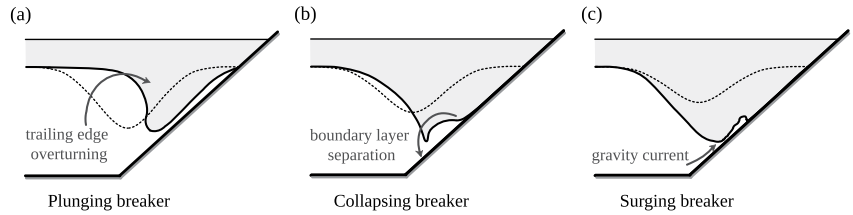

Figure 1. Sketch of the three breaking mechanisms for internal solitary waves (ISWs): (a) plunging, (b) collapsing, and (c) surging breakers. Arrows schematize the main instabilities occurring for each breaker-type. Dotted lines show incident waves before shoaling and breaking.

where $S_w = A_w/\lambda_w$, with A_w wave amplitude and $\lambda_w = S/A_w$ characteristic wavelength, with S wave surface. Boegman et al. (2005) modeled the reflectance coefficient R as a function of Ir, also attempting to relate the Iribarren number to the values for ϵ obtained by Michallet and Ivey (1999).

Broadening the parameter range that was explored in previous experiments, La Forgia, Adduce, and Falcini (2018) found that, for plunging breakers ($Ir < 1$), a dominant steepening of the trailing edge of the wave (Sutherland et al., 2013), followed by a quick clockwise overturning in the onshore direction, induces strong local mixing (Figure 1a). For collapsing breakers (Ir between 1 and 1.5), the trapped dense fluid leaves its original position with a fast downward motion in the adverse pressure gradient region, and a turbulent separated bolus forms and quickly dissipates (Figure 1b). Then, part of the incident wave is reflected and a gravity current composed by the denser fluid flows up the slope, until hydrostatic conditions are reestablished (Aghsaee & Boegman, 2015; la Forgia, Tokyay, Adduce, & Constantinescu, 2020). An intermediate breaking mechanism, that is, the plunging-collapsing breaker, was also observed when the two main shoaling processes occur in the breaking location (i.e., for $Ir \simeq 1$). Finally, in the case of surging breakers ($Ir > 1.5$), ISWs are not subject to any observable large-scale instability during the shoaling, until the wave trough reaches the sloping bottom (Figure 1c); the wave is almost reflected by the right wall of the tank and a gravity current composed of denser fluid moves up the slope causing mixing (la Forgia, Tokyay, Adduce, & Constantinescu, 2018). Each breaking mechanism is characterized by different effects in terms of mixing, fluid entrainment, and shear stress over the bottom (Aghsaee & Boegman, 2015; la Forgia, Tokyay, Adduce, & Constantinescu, 2020).

Numerical modeling has been used extensively to study shoaling and breaking internal waves on slopes both at the field (Bourgault et al., 2007; Lamb, 2002; Vlasenko & Stashchuk, 2007; Walter et al., 2012) and laboratory scales (Aghsaee et al., 2010; Arthur & Fringer, 2014; Vlasenko & Hutter, 2002; Venayagamoorthy & Fringer, 2007). In particular, Bourgault and Kelley (2007) revisited the laboratory experiments of Michallet and Ivey (1999) using two-dimensional numerical simulations and they proposed a parameterization for R as a function of the Iribarren number Ir for laboratory scale waves without side-wall effects:

$$R \simeq \left(1 - e^{-Ir/\xi_0}\right), \tag{3}$$

with $\xi_0 = 0.78 \pm 0.02$, least squares fitting parameter. Aghsaee et al. (2010) investigated the breaking of fully nonlinear ISWs of depression, shoaling upon a uniformly sloping boundary in a smoothed two-layer density field by using high-resolution two-dimensional simulations. They proposed a parameterization for R similar to that of Bourgault and Kelley (2007) by also considering the energy dissipations between the toe of the slope and the breaking location.

In general, to quantify mixing, all experimental and numerical studies we briefly summarized above analyze the evolution of density and velocity fields. Here, through the Ozmidov and Thorpe lengthscales, we develop a novel expression for the mixing efficiency, valid for plunging, and plunging-collapsing breakers, that is, the breakers type mostly expected in the continental shelf region (Cavaliere et al., 2021; La Forgia, Adduce, & Falcini, 2018). By means of experimental results, we relate the mixing efficiency derived by our heuristic model with the one obtained by a canonical, theoretical definition. This relation allows us to directly estimate the change in the background potential energy induced by each breaking event, as a function of the ISWs features and the inclination of the sloping boundary.

2. Mixing Induced by Breaking ISWs

2.1. Theoretical Background

To mix a stably stratified fluid, energy is required to lift heavy fluid elements and lower light elements. For closed fluid systems, only irreversible, diabatic processes can change the probability density function (p.d.f.) of water column density (Winters et al., 1995). In this context, by defining as *adiabatic* a process in which there is no heat or molecular mass transfer, and as *diabatic* a process that is not adiabatic, Winters et al. (1995) partitioned the changes in potential energy due to diabatic mixing from changes due to adiabatic processes, in order to properly quantify the energetics of mixing. By assuming that the state of the flow is known within a fixed two-dimensional domain D, the instantaneous potential and kinetic energies of a fluid are

$$E_p(t) = g \int_D \rho(x, z, t)\, z \, \mathrm{d}x \, \mathrm{d}z, \tag{4}$$

$$E_k(t) = \frac{\rho_0}{2} \int_D \left(u^2 + w^2\right) \, \mathrm{d}x \, \mathrm{d}z, \tag{5}$$

where ρ is the local instantaneous density field, ρ_0 is a constant reference density, z is the vertical spatial coordinate, u, w are the velocities in the x, z directions, respectively. For adiabatic processes, changes in the fluid potential energy result from the switching of the kinetic energy into potential energy without any diffusive mixing (i.e., no heat or mass transfer occurs). Otherwise, diabatic processes produce the change of the total potential energy of the fluid, induced by irreversible molecular diffusion. The instantaneous volume-integrated *background potential energy* is defined as

$$E_b(t) = g \int_D \rho^*(x, z, t)\, z \, \mathrm{d}x \, \mathrm{d}z, \tag{6}$$

where $\rho^*(x, z, t)$ is the density field in the configuration of the minimum potential energy, obtained by sorting the fluid parcels by an adiabatic volume-conserving rearrangement of ρ. For this reason, it uniquely depends on the pdf of density and thus it is not affected by the instantaneous spatial distribution of density in the flow domain. Mixing of the density field $\rho^*(x, z, t)$ corresponds to a change in the p.d.f. induced by mass diffusion, leading to a reduction of the density variance. Blending of fluid parcels is enhanced by turbulence, which causes the steepening of the scalar gradients and the increasing of the iso-scalar surfaces (Winters & D'Asaro, 1996). Changes in the background potential energy are thus associated with the energy consumed in mixing the fluid and can be used to characterize this process.

The difference between the total potential energy and the background potential energy quantifies the amount of potential energy released in the adiabatic transition from $\rho(x, z, t)$ to $\rho^*(x, z, t)$ without altering the p.d.f. of density. This amount of energy is called *available potential energy* (APE), since it represents the amount of potential energy stored in the fluid when it is not in gravitational equilibrium (Lorenz, 1955):

$$E_a(t) = E_p(t) - E_b(t). \tag{7}$$

The APE (E_a) represents the potential energy released if the fluid were to be adiabatically rearranged to the state of minimum potential energy (Thorpe, 1977). This approach estimates empirically the length scales of turbulent overturning in a stratified turbulent flow and is useful for the analysis of vertical density profiles when density inversions are the result of turbulent stirring. The method consists of rearranging or ordering an observed potential density profile, which may contain inversions, into a stable monotonic profile with no inversions. In practice, by considering n samples of density ρ_n, each of which was observed at depth z_n, the Thorpe displacement is $d_n = z_m - z_n$, where the sample at depth z_n had to be moved to depth z_m to generate the stable profile (Dillon, 1982). The resultant *Thorpe length scale* is the root mean square value of the distances d_n:

$$L_T = \langle d^2 \rangle^{1/2}. \tag{8}$$

L_T can be estimated from fine-scale density profiles (Galbraith & Kelley, 1996; Gargett & Garner, 2008; Park et al., 2014), by using a reordering routine or a sorting algorithm that converts the observed profile into one in which density increases downwards everywhere (Thorpe, 2005).

Strictly related to L_T is the *Ozmidov length scale*, defined as (Dillon, 1982; Ozmidov, 1965; Lumley, 1964; Thorpe, 2005)

$$L_O = \left(\frac{\varepsilon}{N^3}\right)^{1/2}, \tag{9}$$

where ε is the turbulent dissipation rate and N is the buoyancy frequency. L_O provides a measure of the vertical size of the largest eddies that may overturn in stably stratified water. The Ozmidov scale can be derived on dimensional grounds when viscosity is negligible (Dillon, 1982; Osborn, 1980; Ozmidov, 1965; Thorpe, 2005). Dillon (1982) suggested a linear relationship between L_T and L_O (Park et al., 2014):

$$L_O = 0.8(\pm 0.4) L_T. \tag{10}$$

On the other hand, the *Kolmogorov length scale*, given by

$$L_K = \left(\frac{\nu^3}{\varepsilon}\right)^{1/4} \sim \mathrm{Re}^{-3/4} L_O, \tag{11}$$

represents the scale at which viscosity dominates and the turbulent kinetic energy is dissipated into heat. Considering the standard assumptions for stratified turbulence (Davidson, 2015; Davidson et al., 2013; Gregg et al., 2018; Imberger & Boashash, 1986), we notice that Equation 11 relates L_K to L_O through the Reynolds number of the large turbulent motion $\mathrm{Re} = c_w L_O/\nu$, where c_w is the ISW phase speed.

Thus, we can infer that the sizes of the largest and smallest eddies in high Reynolds number turbulence potentially differ by many orders of magnitude.

We finally note that, in order to eliminate the dissipation rate ε, by combining the Kolmogorov length scale in Equation 11 and the Ozmidov scale (Equation 9), we can write:

$$\left(\frac{\nu^3}{L_O^2 N^3}\right)^{1/4} \sim Re^{-3/4} L_O \;\Rightarrow\; L_O^2 \sim \frac{\nu^3 Re^3}{L_O^4 N^3} = \frac{c_w^3}{N^3 L_O}, \tag{12}$$

Therefore, we write the Ozmidov scale as

$$L_O = \frac{c_w}{N}. \tag{13}$$

2.2. Heuristic Model for Mixing Efficiency Estimation

The potential energy change ΔE_p in Equation 1 represents the increase in the irreversible potential energy caused by wave breaking on the slope (Bourgault & Kelley, 2007). Hereafter, we indicate it as ΔE_b, that is, the change in the background potential energy.

We calculate the wave APE considering finite and infinite boundaries of the domain for the case of ISWs in two-layer fluid (see also Blokhina [2009]). We assume that the wave of amplitude A_w is propagating in a two-layer fluid with depths h_1 and h_2, and densities ρ_1 and ρ_2, with $\rho_2 > \rho_1$ (Figure 2), with a symmetric structure with respect to the wave; the horizontal domain along which the ISW propagates is $2l_0$ (corresponding to $l_t - x_0$ in Figure 2). We place the coordinate system at the interface between the two layers, in order to set the center of mass of each layer at half-depth. It results that the background potential energy (Equation 6) is

$$E_b = \int_{-l_0}^{l_0} \mathrm{d}x \int_{-h_2}^{0} g\rho_2 z \,\mathrm{d}z + \int_{-l_0}^{l_0} \mathrm{d}x \int_{0}^{h_1} g\rho_1 z \,\mathrm{d}z = \frac{1}{2}\left(\rho_1 h_1^2 - \rho_2 h_2^2\right) 2l_0. \tag{14}$$

The potential energy E_p of the ISW calculated by Equation 4 is

$$E_p = \int_{-l_0}^{l_0} \mathrm{d}x \int_{-h_2}^{\eta(x)} g\rho_2 z \,\mathrm{d}z + \int_{-l_0}^{l_0} \mathrm{d}x \int_{\eta(x)}^{h_1} g\rho_1 z \,\mathrm{d}z = g\frac{(\rho_2 - \rho_1)}{2} \int_{-l_0}^{l_0} \eta^2(x) \,\mathrm{d}x + E_b, \tag{15}$$

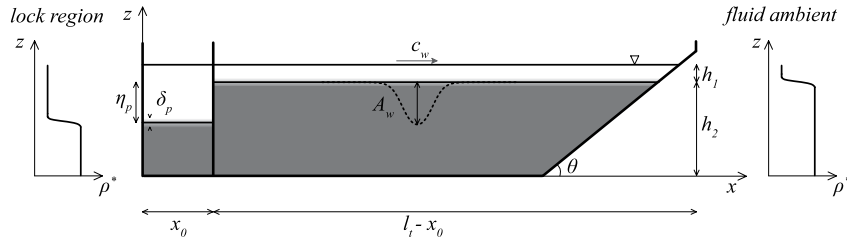

Figure 2. (a) Sketch of the initial experimental setting, and density profiles associated to both the lock region, on the left, and the fluid ambient, on the right. The Perspex wave tank is 3 m long, 0.3 m high, and 0.2 m wide. The lower layer is filled with a solution of sodium chloride (NaCl) with density ρ_2, and the upper layer with fresh water of uniform density $\rho_1 < \rho_2$. the fresh water is dyed by a controlled quantity (0.3 ml/l) of Methylthioninium chloride ($C_{16}H_{18}ClN_3S$). Density of the saline mixture is measured by a density meter (Anton Paar DMA 4100M), with an accuracy of 10^{-1} kg/m^3. A charge-coupled device (CCD) camera placed at a fixed distance from the front wall of the tank is used to record the flow evolution with a frequency of 25 Hz and a spatial resolution of 1,024 × 668 pixels. The resolution of each pixel is approximately 3 × 3 mm.

where $\eta(x)$ is the ISW profile. Thus, the APE of the wave is

$$E_a = \frac{g\Delta\rho}{2}\int_{-l_0}^{l_0} \eta^2(x)\,\mathrm{d}x. \tag{16}$$

Michallet and Ivey (1999) calculate E_0 as

$$E_0 = c_w g\Delta\rho \int_{t_0}^{t_1} \eta^2(t)\,\mathrm{d}t, \tag{17}$$

where t_0 and t_1 are appropriate times, chosen to compute the wave energy. Equation 17 can be rewritten through a change of variable as

$$E_0 = g\Delta\rho\int_{x_1}^{x_2} \eta^2(x)\,\mathrm{d}x \simeq g\Delta\rho\int_{-\infty}^{+\infty} \eta^2(x)\,\mathrm{d}x = 2E_a, \tag{18}$$

where we used relation (Equation 16). We notice in Equation 18 that the integration domain extents to infinity, in order to reach a true APE value (see Hebert [1988] and Lamb [2008] for details).

The APE of an overturn can be defined as $E_a \propto N^2 L_T^2$ (Imberger & Boashash, 1986; Ivey & Imberger, 1991). Given the relationship (10) between L_T and L_O, we find that E_a is highly correlated with the generation of the largest eddies that may overturn in stably stratified water. Therefore, by assuming that most of the incident wave energy is expended to generate an overturn, that is, $E_0 = 2E_a \propto 2\,N^2(L_O^2/0.64)$, we can introduce the *pseudo-mixing efficiency* ϵ_O:

$$\epsilon_O = \frac{\Delta E_b}{2M_w N^2 L_T^2(1-R)} \simeq \frac{\Delta E_b}{2M_w N^2 (L_O/0.8)^2(1-R)} = \frac{\Delta E_b\, 0.64}{2M_w c_w^2(1-R)}, \tag{19}$$

where we introduced the wave mass per unit of width, $M_w \simeq A_w\lambda_w\rho_1$, written in terms of simple geometrical quantities, in order to be dimensionally consistent. In Equation 19, R can be parameterized through Equation 3, as done by Bourgault and Kelley (2007) and Aghsaee et al. (2010).

Equation 19 represents a suitable, heuristic model for diagnosing mixing efficiency from ISW geometrical features. Indeed, we expect (Equation 19) to be correlated to the mixing efficiency (Equation 1). However, (Equation 19) still requires the knowledge of ΔE_b, which we will be evaluated in the next section.We remark that ϵ_O, although dimensionally consistent with ϵ, cannot be rigorously considered as a mixing efficiency. Indeed, it is not obtained in the canonical fashion by estimating the ISW total mechanical energy (e.g., as in Davies Wykes and Dalziel [2014]), but as a function of the main wave geometrical parameters.

Table 1
Experimental Parameters and Internal Solitary Waves (ISWs) Features for the Seven Cases: The Inclination of the Sloping Boundary s, the Undisturbed Layers Thickness h_1 and h_2, the ISWs Amplitude A_w, the Wavelength λ_w, the ISWs Celerity c_w, the Incident ISWs Energy $E_{0,inc}$ and the Reflectance Coefficient R

Case	s	h_1 (m)	h_2 (m)	A_w (m)	λ_w (m)	c_w (m/s)	$E_{0,inc}$ (J/m)	R
1	0.291	0.0111	0.1990	0.043	0.248	0.112	9.029×10^{-2}	0.318
2	0.292	0.0117	0.1984	0.020	0.166	0.105	1.329×10^{-2}	0.464
3	0.173	0.0082	0.1218	0.028	0.165	0.091	2.641×10^{-2}	0.205
4	0.158	0.0075	0.1225	0.032	0.139	0.105	3.076×10^{-2}	0.152
5	0.249	0.0075	0.1225	0.030	0.133	0.102	2.453×10^{-2}	0.223
6	0.194	0.0075	0.1225	0.028	0.130	0.100	2.070×10^{-2}	0.225
7	0.268	0.0075	0.1225	0.029	0.145	0.096	2.602×10^{-2}	0.238

3. Model Validation and Prediction of the Mixing Efficiency

3.1. Experimental and Numerical Assessment

To diagnose Equation 19 we performed laboratory experiments, generating ISWs by the standard lock-release method in a two-layer stratified system (Kao et al., 1985; La Forgia, Adduce, & Falcini, 2018). Initially, at a distance x_0 from the left wall of the tank, a 4 mm thick, vertical and removable Perspex gate separates the lock fluid, on the left hand-side of the tank, from the ambient fluid on the right ($l_t - x_0$ in Figure 2). For each side of the tank, a stratified two-layer distribution is obtained by filling the lower layer with a solution of density ρ_2 and depth h_2, and the upper layer with fresh water of uniform density $\rho_1 < \rho_2$ and depth $h_1 < h_2$. This particular setting is aimed to reproduce ISWs of depression, the most common type of ISWs detected in the coastal areas (Alpers et al., 2008; Duda et al., 2004; Helfrich & Melville, 2006; Jackson et al., 2013; Osborne & Burch, 1980), where the stratification shows a relatively thin upper layer. Before each run, we measure the density of the saline mixture in order to make sure that the density difference between the two uniform layers is of 30 kg/m^3. Indeed, in the coastal ocean, the typical value of the Boussinesq parameter, that is, the ratio of the density difference between the two layers and a reference density, is about 0.03 (Chen et al., 2007). We observe that, for this value, the effects of the disturbances at the free surface are negligible, and do not have significant impact on the induced mixing (Kodaira et al., 2016; la Forgia & Sciortino, 2019). The different depths of the pycnoclines of the two stratifications produces the interfacial displacement η_P; a sloping boundary, making an angle θ with the horizontal, is placed on the right hand-side of the tank to induce the ISWs breaking and partial reflection (Figure 2). All experiments start with the gate removal and the consequent gravity collapse: an ISW of depression generates and propagates downstream.

We perform seven runs, characterized by different initial conditions in order to generate ISWs having different geometric and kinematic features (see Table 1). By varying the inclination of the sloping boundary we force the ISWs to break as plunging breakers (La Forgia, Adduce, & Falcini, 2018), that is, with Iribarren numbers ranging from 0.33 to 0.84. Using dye as tracer we derive, for each image pixel, a relation between the amount of uniformly distributed dye in the tank and the gray scale values. Those relations are obtained by acquiring, at the end of each experiment, several images, each characterized by a fixed concentration of dye (la Forgia, Ottolenghi, et al., 2020; Ottolenghi, Adduce, Inghilesi, Armenio, & Roman, 2016; Theiler & Franca, 2016). The evaluation of the instantaneous density fields has an accuracy of about 0.1 kg/m^3 (i.e., the ratio between the maximum range of density and the gray scale levels).

The normalized density $\rho^*(x, z, t)$ is given by:

$$\rho^*(x, z, t) = \frac{\rho(x, z, t) - \rho_1}{\rho_2 - \rho_1}, \tag{20}$$

where x and z represent the streamwise and vertical directions (Figure 2), t is the time since the gate removal, and ρ^* ranges between 0 (fresh upper layer) and 1 (salty lower layer).

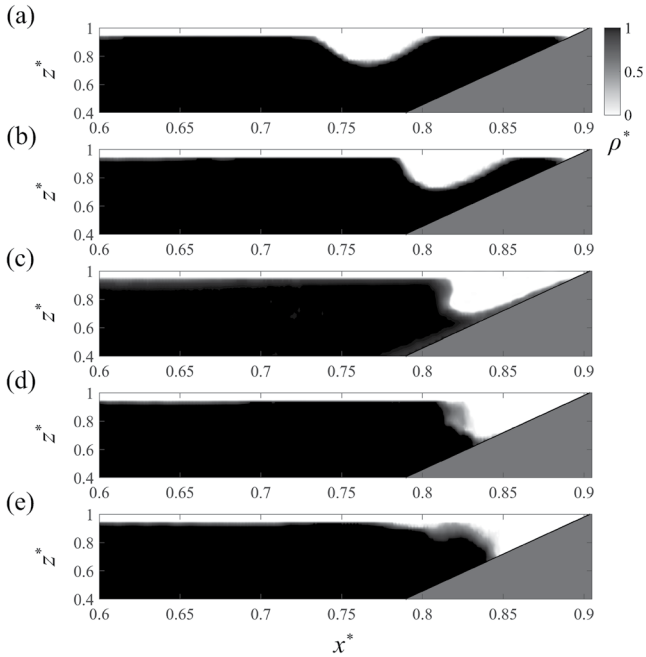

Figure 3. ISW breaking evolution during the interaction with the sloping boundary for Case 6 (see Table 1).

The analysis of the density fields allows us to infer the pycnocline thickness δ_P (Figure 2) and the instantaneous pycnocline position that is associated to the iso-density level $\rho^*(x, z, t) = 0.5$. For all cases, we derive an initial pycnocline thickness δ_{Pi} of 1 cm. However, in general, the pycnocline thickness does not affect the ISW geometrical features and the breaking mechanism (la Forgia, Ottolenghi, et al., 2020; Sutherland et al., 2013). Then, we derive the ISW amplitude A_w, surface S_w, and celerity c_w (i.e., the first derivative of the trough's position). The characteristic wavelength λ_w is estimated as (Michallet & Ivey, 1999):

$$\lambda_w = \frac{1}{A_w}\int_{-\infty}^{+\infty} \eta(x)\,\mathrm{d}x = \frac{S_w}{A_w} \tag{21}$$

where $\eta(x)$ is the pycnocline displacement along the domain. Being $L = 3$ m the length of the tank, $H = h_1 + h_2$ the total water depth, $g' = g(\rho_2 - \rho_1)/\rho$ the reduced gravity, and $u_b = \sqrt{g'\,H}$ the buoyancy velocity, we herein consider the normalized quantities $x^* = x/L$, $z^* = z/H$, and $t^* = t\,H/u_b$ to analyze the spatiotemporal evolution of the performed experiments in a dimensionless form.

The gravity collapse, induced by the gate removal, causes the generation of an ISW of depression (Figure 3) that propagates with approximately constant celerity, amplitude, and wavelength (as proved by the white strip at $1.5 < t^* < 3.5$ in Figure 4a for Case 5). The incident ISW approaches the sloping boundary, where it shoals and breaks (Figure 3). The wave breaking develops with the trailing edge overturning, which induces mixing and partial reflection: a train of four, rank-ordered ISWs are indeed observed to propagate upstream, toward the lock region (Figure 4c for Case 5). The Hovmöller diagram shows that the reflected ISWs celerity is proportional to their size (see Figure 4a at $5 < t^* < 9$). For all experiments, the train of reflected waves is composed by four ISWs.

To estimate the energy released at the sloping region, and thus to obtain the change of background potential energy (ΔE_b) in Equation 19, we evaluate the difference between the incident and the reflected ISWs energy. To avoid that experimental inaccuracies (e.g., camera resolution) may affect the evaluation of the instantaneous

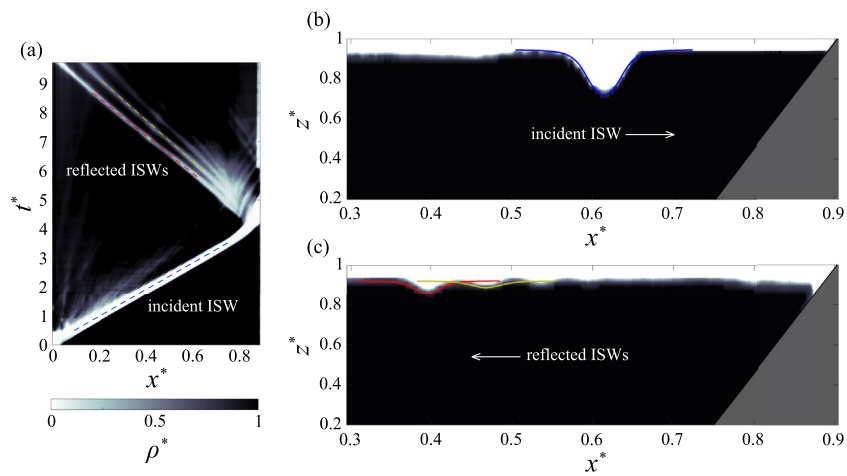

Figure 4. Experimental Case 5: (a) Hovmöller diagram in the plane (x^*, t^*) associated to the horizontal plane at $z^* = 0.915$; dashed blue line indicates incident wave, red and yellow lines indicate the first two reflected ISWs. (b) Density field at $t^* = 2.89$, and the ISW profile predicted by the Dubreil-Jacotin-Long (DJL) model for the incident wave approaching the sloping boundary (blue line); (c) density field at $t^* = 7.22$ showing the train of ISWs reflected upstream, after the incident ISW breaking. Red and yellow lines show the ISW profile predicted by the DJL model for the first two reflected ISWs. The reflected ISWs propagate through a stratified ambient with a density distribution reported in Figure 2.

pycnocline position, and thus of wave geometrical features and ISW energies, we derive the $\rho^* = 0.5$ iso-density line from the fully nonlinear and strongly dispersive DJL model (Dubreil-Jacotin, 1937; Dunphy et al., 2011; Long, 1953; Turkington et al., 1991; Xu & Stastna, 2019). This synergy between experimental runs and the DJL model allows us to obtain the instantaneous pycnocline position also for smaller waves, characterized by pycnocline displacements comparable to the pixel size.

For stratified flows, numerical solutions for ISWs can be derived from a nonlinear elliptic eigenvalue problem for $\eta(x, z)$, that is, the DJL equation

$$\nabla^2\eta + \frac{N^2(z-\eta)}{c_w^2}\eta = 0, \tag{22a}$$

$$\eta = 0 \text{ at } z = 0, H \tag{22b}$$

$$\eta \to 0 \text{ as } x \to \pm\infty. \tag{22c}$$

Solutions of Equation 22a represents exact solutions of Euler's equations, and they are derived by a generalization of a variational technique and a numerical algorithm (Dunphy et al., 2011; Turkington et al., 1991). In this algorithm neither the wave amplitude, nor the wave propagation speed are specified. Whereas, the kinetic energy of the disturbance is minimized under the constraint that the available potential energy (scaled by $\rho_0 gH$)

$$\text{APE}(\eta) = \frac{1}{H}\int_0^H\int_{-\infty}^{+\infty}\int_0^{\eta}[\bar{\rho}(z-\eta) - \bar{\rho}(z-s)]\,\mathrm{d}s\,\mathrm{d}x\,\mathrm{d}z, \tag{23}$$

is held fixed (Dunphy et al., 2011; Xu & Stastna, 2019), with $\bar{\rho}$ density profile scaled by the reference density ρ_0.

For each ISW, we set the DJL model by imposing the density profile measure in the tank experiment, and by tuning the wave APE in order to obtain, numerically, the experimental ISW amplitudes (e.g., see red line in Figure 4b for Case 5 incident ISW and red and yellow lines in Figure 4c for the first two reflected ISWs). From the DJL solutions for the pycnocline displacements, we evaluate ISWs energies through Equation 18. The total reflected ISWs energy E_R, associated to the train of n reflected waves, is obtained as the sum of the single energetic contribution of each ISW, that is, $E_R = \sum_i E_{Ri}$, with $i = 1, \ldots, n$.

Once derived the energy released over the breaking location, we estimate the effective amount of this energy lost for mixing processes. To quantify mixing induced by ISWs breaking, we adopt the energy budget method of Winters et al. (1995), which has been widely used in literature (Fragoso et al., 2013; la Forgia, Tokyay, Adduce, & Constantinescu, 2018; Ottolenghi, Adduce, Inghilesi, Armenio, & Roman, 2016; Ottolenghi, Adduce, Inghilesi, Roman, & Armenio, 2016; Patterson et al., 2006). For each case, we estimate the change in the background potential energy (ΔE_b) between the initial condition, associated to the ISW that is approaching the sloping boundary, and a final condition associated to the release of all the reflected waves. This allows us to exclude mixing induced by the generation mechanism, and to consider the effective change in the background potential energy produced by the breaking process.

3.2. Estimation of the Mixing Efficiency

For each experiment, we estimate both mixing efficiency that is obtained from laboratory experiments (ϵ), that is, directly from Equation 1, and the one we derive from the heuristic model (ϵ_O) in Equation 19. In particular, we estimate the ISWs features, that is, A_w, M_w, c_w, and λ_w, and their energies E_0 and E_R through image analysis of the laboratory experiments and the DJL model. The change of the background potential energy (ΔE_b) is estimated from the resulting density fields by using image analysis (Winters et al., 1995).

To validate and extend our results to a larger number of cases, we consider also experimental results obtained by Michallet and Ivey (1999), who followed a laboratory technique similar to the one we adopt for our cases. These authors used two probes, placed in the wave tank to measure the density profiles nearby the sloped surface. Then they evaluated the change in the total potential energy (ΔE_p) occurring in the trapezoidal region upstream the sloping boundary. They compared, in particular, the total potential energy before and after the breaking event, such as the fluid confined within the considered domain is at rest, and the total available potential energy is

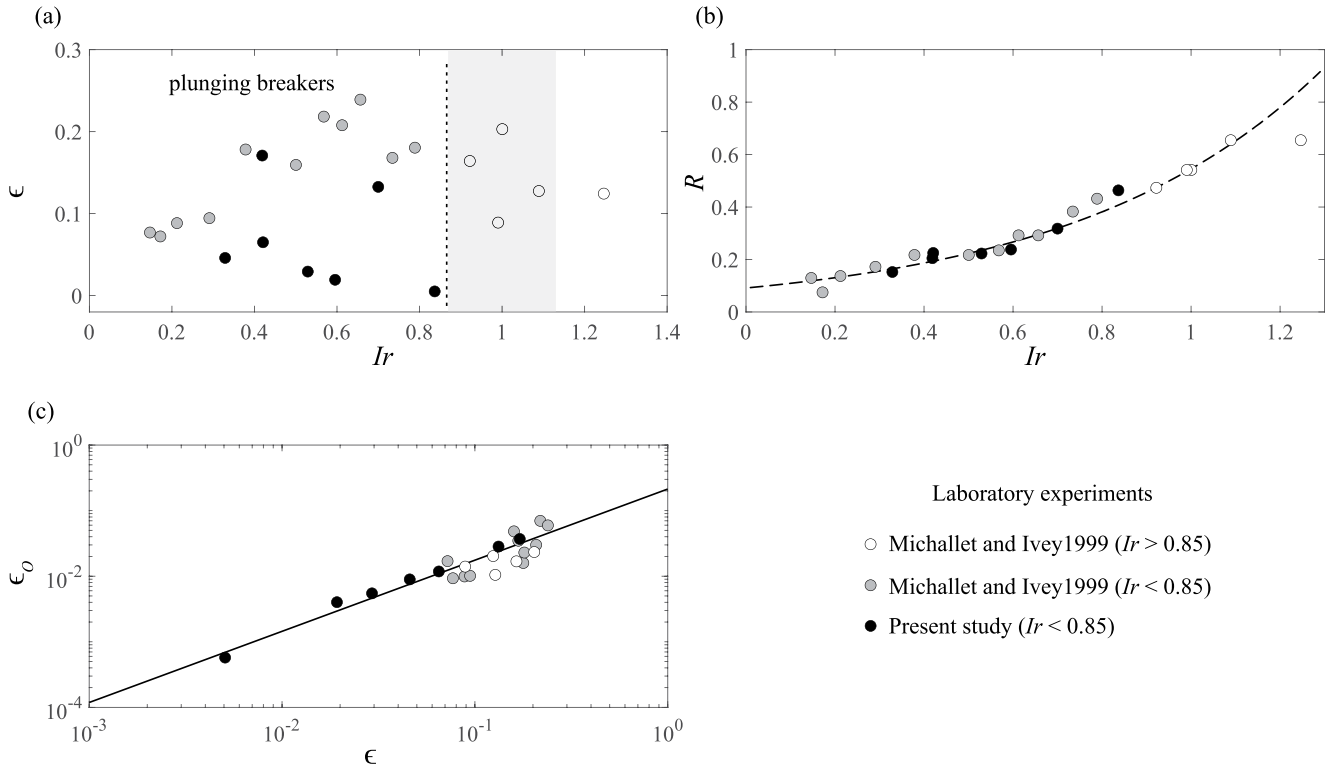

Figure 5. (a) Relation between the Iribarren number (Ir) and the experimental mixing efficiency (ϵ). Shaded region highlights the plunging-collapsing breakers domain, while larger Ir are associated to the surging breakers domain. (b) Ir versus the reflectance parameter (R), and the associated fitting exponential curve (dashed line); (c) log-log plot of ϵ versus the mixing efficiency derived by our heuristic model. Experiments from the present work and from Michallet and Ivey (1999) are reported.

zero (i.e., $\Delta E_b = \Delta E_p$). Considered the non-uniform density distribution along the x-direction, we argue that the estimation of E_b from experimental density fields provides larger values of potential energy with respect to those obtained by local probe measurements.

Despite these methodological differences, the reflectance parameter $R = E_R/E_0$ obtained by our experimental and numerical analysis is related with the internal Iribarren number, and it follows the same trend discussed by Michallet and Ivey (1999) (Figure 5b). They estimated the reflected energy by considering the only contribution of the leading off-shore propagating ISW, assuming that the energy related to the following waves is negligible. The large coefficient of correlation (R^2_{corr}) of the exponential function relating Ir and R (i.e., Equation 24) suggests that the internal Iribarren number is a valid predictive parameter of the reflected wave energy:

$$R = 0.0913\, e^{1.787\, Ir}, \quad R^2_{corr} = 0.93. \tag{24}$$

However, in agreement with the results obtained by Michallet and Ivey (1999) and Arthur and Fringer (2014), there is not a feasible relation between Ir and the experimental mixing efficiency (Figure 5a). The internal Iribarren number is, indeed, a dimensionless parameter able to identify the different breaking mechanisms that may occur when an ISW shoals upon a sloping boundary, but it is not suitable to identify the amount of mixing induced by wave breaking. Parameters that define Ir only consider ISWs and sloping boundary main geometrical properties (i.e., A_w, λ_w, and s) and they do not account for either any energetic parameter or stratification effects. Our results confirm that mixing efficiency is not solely related to the Iribarren number. This means that mixing cannot be uniquely predicted from wave geometry but also ISW energetics must be considered.

In seeking to define a predictive tool for mixing efficiency, we compare results from laboratory experiments to those we derived from heuristic model (Figure 5a). Since our model takes into account only plunging breakers, besides all our cases (black solid dots in Figure 5), we consider a selected group of runs performed by Michallet

and Ivey (1999), characterized by $Ir < 0.85$ (gray solid dots in Figure 5). The resulting relation between ϵ and ϵ_O can be described by the power law

$$\epsilon_O = 0.214\,\epsilon^{1.085} \quad R^2_{corr} = 0.90, \tag{25}$$

which confirms that our parametrization can be considered a valid approximation to describe mixing efficiency induced by plunging and plunging-collapsing breakers.

Data associated to larger ϵ show a larger scattering that could be associated to the different approach adopted by Michallet and Ivey (1999) to estimate ΔE_b and to evaluate the reflected energy.

Interestingly, although we obtain the power law from data that are characterized by $Ir < 0.85$, also plunging-collapsing breakers (i.e., the ones with $Ir > 0.85$) show a relatively good agreement with Equation 25. This suggests that the bulk mixing is largely affected by the overturning of the ISWs trailing edge, rather than by the boundary layer separation occurring close to the sloping bottom, associated to the collapsing breakers. For this reason, our results can be considered valid for a slightly wider range of Ir values (i.e., for $Ir \to 1.5$).

The relation between ϵ and ϵ_O allows us to directly derive the change in the background potential energy once the undisturbed stratification, ISWs geometry, and topographic features (Ir, M_w, and E_0) are known:

$$\Delta E_b = (1 - R)\left[\frac{E_0^{1.085}}{0.667\, c_w^2\, M_w}\right]^{11.752}. \tag{26}$$

By estimating ΔE_b, it is therefore possible to derive the expected mixing efficiency as $\epsilon = \Delta E_b/[E_0(1 - R)]$ without directly evaluating the evolution of the density field during the breaking event. Although the variation of pycnocline thicknesses does not affect the breaking mechanism (i.e., ISWs geometrical features), we observe that for weaker stratifications, slower waves are expected. The wave celerity, indeed, represents a scaling factor for the wave energy (see Equation 17) and, consequently, for the mixing efficiency (see Equation 26). This means that for faster waves, lower values for the mixing efficiency will occur. Our heuristic model takes into account stratification effects in terms of wave celerity in the definition of the pseudo-mixing efficiency (Equation 19). We thus can consider the pseudo-mixing efficiency as representative of all possible density distributions characterized by layer depths $h_1 < h_2$ (i.e., for ISWs of depression).

Internal waves over topographic constraints enhance fine-scale shear and strain over rough bathymetry (Artale et al., 2018; Polzin et al., 1997). In particular, internal waves breaking induces an expansion of energy that results in mixing the stratified fluid and, consequently, causes upwelling of abyssal waters along sloping boundaries (Ferrari et al., 2016; Wunsch & Ferrari, 2004). We note that our estimation of mixing efficiency, based on the knowledge of both ISW and topographic geometries a priori, expands the ability to parametrize fine-scale shear and strain processes that are crucial for the diagnosis of diapycnal mixing and, in general, ocean heat content conundrum (Artale et al., 2018; McDougall & Ferrari, 2017).

Fields observations show strong evidence of large amplitude ISWs propagating in two-layer configurations, interacting with a sloped seafloor. To compare our results with those obtained in previous studies we finally test our model for some real-field cases. In particular, we consider ISWs breaking occurring in the following locations: Seneca Lake (Hunkins & Fliegel, 1973), State of New York, US; Lock Ness (Thorpe, 1974), Scottish Highlands; Sulu Sea (Apel et al., 1985), southwestern area of the Philippines. For these cases, Michallet and Ivey (1999) provide values of mixing efficiency associated to individual breaking events, using physical parameters described in previous literature. In particular, they obtained the following values for ϵ: 0.18 (Seneca Lake), 0.13 (Loch Ness), 0.10 (Sulu Sea). We test our model on these cases, evaluating $\epsilon = \Delta E_b/(E_0(1 - R))$, with ΔE_b as in Equation 26, and E_0 calculated from Equation 18 with $\eta(x)$ derived from the DJL model. We obtain a mixing efficiency of 0.17, 0.08, and 0.03, respectively. This suggests that our heuristic model reproduce a similar trend although underestimating the mixing efficiency with respect to the results obtained by Michallet and Ivey (1999). Our model could represent a promising tool to evaluate the mixing efficiency trend, although a rigorous comparison with real-field observations, aimed at deriving more precise values for ϵ, should be carried out. However, we expect our approach to conveniently capture the variability in mixing efficiency for ISWs with different geometrical features. In particular, this can be useful for studying the mixing effects of ISWs with different features breaking in a single specifying location.

4. Conclusions

For stratified flows, prediction of changes in kinetic and background potential energies represents the main challenge for estimating mixing, without directly evaluate instantaneous density and velocity fields by experimental studies, numerical modeling or real field observations.

In the present paper, we develop a synergy of laboratory experiments, numerical modeling and theoretical analysis, deriving a predictive tool for the mixing efficiency induced by breaking ISWs over a sloping boundary. The different ISWs breaking mechanisms are usually identified by the internal Iribarren number. However, it is not possible to derive a relation between waves and topography geometrical features and the associated mixing. Our theoretical approach is based on the available potential energy associated to the ISW and on specific turbulent scales, that is, Ozmidov and Thorpe lengthscales. Starting from the definition provided by Helfrich (1992) and Michallet and Ivey (1999), we obtain a heuristic expression for the mixing efficiency (pseudo-mixing efficiency, ϵ_O), assuming that all the incident ISW energy is involved in the overturning event. This is the expected breaking behavior for plunging and plunging-collapsing breakers, in response to the verticalization of the trailing wave edge as the ISW shoals over the sloping boundary. The relationship shows that the pseudo-mixing efficiency depends on both the change of the background potential energy (ΔE_b) and on the net wave energy (i.e., $E_0(1-R)$) involved in the mixing process. In particular, the incident energy E_0 appears to be well represented by the product of the wave mass and the squared wave celerity. We estimate mixing by both the canonical and the heuristic expressions for a set of laboratory experiments performed in order to widen the range of Iribarren number investigated by Michallet and Ivey (1999). The relation between ϵ and ϵ_O is well approximated by a power law, with a good degree of correlation. This relationship allows us to directly estimate the change in the background potential energy, without a direct evaluation of the density field evolution. Indeed, it is possible to derive ΔE_b once the undisturbed stratification, ISWs geometry, and topographic features are known (Ir, M_w, and E_0). By testing our results for real field conditions, we found that our approach provides values of mixing efficiency close to those previously estimated for oceanographic cases, and, in particular, it captures the same trend. Therefore, the developed model represents a suitable predicting tool for estimation of ISWs-driven diapycnal mixing in the coastal oceans, expanding the ability to parametrize fine-scale shear and strain processes (Artale et al., 2018; McDougall & Ferrari, 2017).

Data Availability Statement

Experimental data are publicly available at https://doi.org/10.6084/m9.figshare.13656512.v1.

Acknowledgments
This work was partially supported by EMODnet (European Marine Observation and Data Network Physics), and the Flagship Project RITMARE (The Italian Research for the Sea), coordinated by the Italian National Research Council and funded by the Italian Ministry of Education, University and Research. Open Access Funding provided by Consiglio Nazionale delle Ricerche within the CRUI-CARE Agreement.

References

Aghsaee, P., & Boegman, L. (2015). Experimental investigation of sediment resuspension beneath internal solitary waves of depression. *Journal of Geophysical Research: Oceans*, *120*(5), 3301–3314. https://doi.org/10.1002/2014jc010401

Aghsaee, P., Boegman, L., & Lamb, K. G. (2010). Breaking of shoaling internal solitary waves. *Journal of Fluid Mechanics*, *659*, 289–317. https://doi.org/10.1017/s002211201000248x

Alpers, W., Brandt, P., & Rubino, A. (2008). Internal waves generated in the Straits of Gibraltar and Messina: Observations from space. In *Remote sensing of the European seas* (pp. 319–330). Springer.

Apel, J. R., Holbrook, J. R., Liu, A. K., & Tsai, J. J. (1985). The Sulu Sea internal soliton experiment. *Journal of Physical Oceanography*, *15*(12), 1625–1651. https://doi.org/10.1175/1520-0485(1985)015<1625:tssise>2.0.co;2

Artale, V., Falcini, F., Marullo, S., Bensi, M., Kokoszka, F., Iudicone, D., & Rubino, A. (2018). Linking mixing processes and climate variability to the heat content distribution of the Eastern Mediterranean abyss. *Scientific Reports*, *8*, 11317. https://doi.org/10.1038/s41598-018-29343-4

Arthur, R. S., & Fringer, O. B. (2014). The dynamics of breaking internal solitary waves on slopes. *Journal of Fluid Mechanics*, *761*, 360–398. https://doi.org/10.1017/jfm.2014.641

Barry, M., Ivey, G. N., Winters, K., & Imberger, J. (2001). Measurements of diapycnal diffusivities in stratified fluids. *Journal of Fluid Mechanics*, *442*, 267–291. https://doi.org/10.1017/s0022112001005080

Blokhina, M. (2009). *Shoaling internal solitary waves* (Ph.D. Thesis). Memorial University of Newfoundland.

Boegman, L., Ivey, G., & Imberger, J. (2005). The degeneration of internal waves in lakes with sloping topography. *Limnology and Oceanography*, *50*(5), 1620–1637. https://doi.org/10.4319/lo.2005.50.5.1620

Boegman, L., & Stasna, M. (2019). Sediment resuspension and transport by internal solitary waves. *Annual Reviews of Fluid Mechanics*, *51*, 129–154. https://doi.org/10.1146/annurev-fluid-122316-045049

Bogucki, D., Dickey, T., & Redekopp, L. G. (1997). Sediment resuspension and mixing by resonantly generated internal solitary waves. *Journal of Physical Oceanography*, *27*(7), 1181–1196. https://doi.org/10.1175/1520-0485(1997)027<1181:srambr>2.0.co;2

Bouffard, D., & Boegman, L. (2013). A diapycnal diffusivity model for stratified environmental flows. *Dynamics of Atmospheres and Oceans*, *61–62*, 14–34. https://doi.org/10.1016/j.dynatmoce.2013.02.002

Bourgault, D., Blokhina, M. D., Mirshak, R., & Kelley, D. E. (2007). Evolution of a shoaling internal solitary wavetrain. *Geophysical Research Letters*, *34*(3), L03601. https://doi.org/10.1029/2006gl028462

Bourgault, D., & Kelley, D. E. (2007). On the reflectance of uniform slopes for normally incident interfacial solitary waves. *Journal of Physical Oceanography*, *37*(5), 1156–1162. https://doi.org/10.1175/jpo3059.1

Brandt, P., Rubino, A., Quadfasel, D., Alpers, W., Sellschopp, J., & Fiekas, H.-V. (1999). Evidence for the influence of Atlantic–Ionian stream fluctuations on the tidally induced internal dynamics in the Strait of Messina. *Journal of Physical Oceanography*, *29*(5), 1071–1080. https://doi.org/10.1175/1520-0485(1999)029<1071:eftioa>2.0.co;2

Cacchione, D. A., Pratson, L. F., & Ogston, A. S. (2002). The shaping of continental slopes by internal tides. *Science*, *296*(5568), 724–727. https://doi.org/10.1126/science.1069803

Cavaliere, D., la Forgia, G., Adduce, C., Alpers, W., Martorelli, E., & Falcini, F. (2021). Breaking location of internal solitary waves over a sloping seabed. *Journal of Geophysical Research: Oceans*, *126*(2), e2020JC016669. https://doi.org/10.1029/2020jc016669

Chen, C.-Y., Hsu, J. R.-C., Chen, C.-W., Chen, H.-H., Kuo, C.-F., & Cheng, M.-H. (2007). Generation of internal solitary wave by gravity collapse. *Journal of Marine Science and Technology*, *15*(1), 1–7.

Choi, W., & Camassa, R. (1999). Fully nonlinear internal waves in a two-layer fluid system. *Journal of Fluid Mechanics*, *396*, 1–36. https://doi.org/10.1017/s0022112099005820

Davidson, P. (2015). *Turbulence: An introduction for scientists and engineers*. Oxford University Press.

Davidson, P., Kaneda, Y., & Sreenivasan, K. (2013). *Ten chapters in turbulence*. Cambridge University Press.

Davies Wykes, M. S., & Dalziel, S. B. (2014). Efficient mixing in stratified flows: Experimental study of a Rayleigh–Taylor unstable interface within an otherwise stable stratification. *Journal of Fluid Mechanics*, *756*, 1027–1057. https://doi.org/10.1017/jfm.2014.308

Davis, K. A., & Monismith, S. G. (2011). The modification of bottom boundary layer turbulence and mixing by internal waves shoaling on a barrier reef. *Journal of Physical Oceanography*, *41*(11), 2223–2241. https://doi.org/10.1175/2011jpo4344.1

Dillon, T. M. (1982). Vertical overturns: A comparison of Thorpe and Ozmidov length scales. *Journal of Geophysical Research*, *87*(C12), 9601–9613. https://doi.org/10.1029/jc087ic12p09601

Droghei, R., Falcini, F., Casalbore, D., Martorelli, E., Mosetti, R., Sannino, G., & Chiocci, F. (2016). The role of internal solitary waves on deep-water sedimentary processes: The case of up-slope migrating sediment waves off the Messina Strait. *Scientific Reports*, *6*, 36376. https://doi.org/10.1038/srep36376

Dubreil-Jacotin, M. L. (1937). Sur les theoremes d'existence relatifs aux ondes permanentes periodiques a deux dimensions dans les liquides heterogenes. *Journal de Mathematiques Pures et Appliquees*, *16*, 43–67.

Duda, T. F., Lynch, J. F., Irish, J. D., Beardsley, R. C., Ramp, S. R., Chiu, C.-S., et al. (2004). Internal tide and nonlinear internal wave behavior at the continental slope in the northern South China Sea. *IEEE Journal of Oceanic Engineering*, *29*(4), 1105–1130. https://doi.org/10.1109/joe.2004.836998

Dunphy, M., Subich, C., & Stastna, M. (2011). Spectral methods for internal waves: Indistinguishable density profiles and double-humped solitary waves. *Nonlinear Processes in Geophysics*, *18*(3), 351–358. https://doi.org/10.5194/npg-18-351-2011

Ferrari, R., Mashayek, A., McDougall, T. J., Nikurashin, M., & Campin, J. M. (2016). Turning ocean mixing upside down. *Journal of Physical Oceanography*, *46*(7), 2239–2261. https://doi.org/10.1175/jpo-d-15-0244.1

Ferron, B., Mercier, H., Speer, K., Gargett, A., & Polzin, K. (1998). Mixing in the Romanche fracture zone. *Journal of Physical Oceanography*, *28*, 1929–1945. https://doi.org/10.1175/1520-0485(1998)028<1929:mitrfz>2.0.co;2

Fragoso, A., Patterson, M., & Wettlaufer, J. S. (2013). Mixing in gravity currents. *Journal of Fluid Mechanics*, *734*. https://doi.org/10.1017/jfm.2013.475

Galbraith, P. S., & Kelley, D. E. (1996). Identifying overturns in CTD profiles. *Journal of Atmospheric and Oceanic Technology*, *13*(3), 688–701. https://doi.org/10.1175/1520-0426(1996)013<0688:ioicp>2.0.co;2

Gargett, A., & Garner, T. (2008). Determining Thorpe scale from ship-lowered CTD density profiles. *Journal of Atmospheric and Oceanic Technology*, *25*(9), 1657–1670. https://doi.org/10.1175/2008jtecho541.1

Gregg, M., D'Asaro, E., Riley, J., & Kunze, E. (2018). Mixing efficiency in the ocean. *Annual Review of Marine Science*, *10*, 443–473. https://doi.org/10.1146/annurev-marine-121916-063643

Grimshaw, R., Pelinovsky, E., Talipova, T., & Kurkin, A. (2004). Simulation of the transformation of internal solitary waves on oceanic shelves. *Journal of Physical Oceanography*, *34*(12), 2774–2791. https://doi.org/10.1175/jpo2652.1

Grimshaw, R., Pelinovsky, E., Talipova, T., & Kurkina, O. (2010). Internal solitary waves: Propagation, deformation, disintegration. *Nonlinear Processes in Geophysics*, *17*(6), 633–649. https://doi.org/10.5194/npg-17-633-2010

Grue, J. (2006). Very large internal waves in the ocean - Observations and nonlinear models. In J. Grue & K. Trulsen (Eds.), *Waves in geophysical fluids: Tsunamis, rogue waves, internal waves and internal tides* (pp. 205–270). SpringerWienNewYork.

Hebert, D. (1988). The available potential energy of an isolated feature. *Journal of Geophysical Research*, *93*(C1), 556–564. https://doi.org/10.1029/jc093ic01p00556

Helfrich, K. R. (1992). Internal solitary wave breaking and run-up on a uniform slope. *Journal of Fluid Mechanics*, *243*, 133–154. https://doi.org/10.1017/s0022112092002660

Helfrich, K. R., & Melville, W. K. (2006). Long nonlinear internal waves. *Annual Review of Fluid Mechanics*, *38*, 395–425. https://doi.org/10.1146/annurev.fluid.38.050304.092129

Hunkins, K., & Fliegel, M. (1973). Internal undular surges in Seneca Lake: A natural occurrence of solitons. *Journal of Geophysical Research*, *78*(3), 539–548. https://doi.org/10.1029/jc078i003p00539

Imberger, J., & Boashash, B. (1986). Application of the Wigner–Ville distribution to temperature gradient microstructure: A new technique to study small–scale variations. *Journal of Physical Oceanography*, *16*(12), 1997–2012. https://doi.org/10.1175/1520-0485(1986)016<1997:aotwdt>2.0.co;2

Ivey, G. N., & Imberger, J. (1991). On the nature of turbulence in a stratified fluid. Part I: The energetics of mixing. *Journal of Physical Oceanography*, *21*(5), 650–658. https://doi.org/10.1175/1520-0485(1991)021<0650:otnoti>2.0.co;2

Ivey, G. N., Winters, K., & Koseff, J. (2008). Density stratification, turbulence, but how much mixing? *Annual Reviews of Fluid Dynamics*, *40*, 169–184. https://doi.org/10.1146/annurev.fluid.39.050905.110314

Jackson, C. R., Da Silva, J. C. B., Jeans, G., Alpers, W., & Caruso, M. J. (2013). Nonlinear internal waves in synthetic aperture radar imagery. *Oceanography*, *26*(2), 68–79. https://doi.org/10.5670/oceanog.2013.32

Kao, T. W., Pan, F.-S., & Renouard, D. (1985). Internal solitons on the pycnocline: Generation, propagation, and shoaling and breaking over a slope. *Journal of Fluid Mechanics*, *159*, 19–53. https://doi.org/10.1017/s0022112085003081

Klymak, J., Pinkel, R., & Rainville, L. (2008). Direct breaking of the internal tide near topography: Kaena Ridge, Hawaii. *Journal of Physical Oceanography*, *38*(2), 380–399. https://doi.org/10.1175/2007jpo3728.1

Kodaira, T., Waseda, T., Miyata, M., & Choi, W. (2016). Internal solitary waves in a two-fluid system with a free surface. *Journal of Fluid Mechanics*, *804*, 201–223. https://doi.org/10.1017/jfm.2016.510

Kokoszka, F., Falcini, F., Iudicone, D., Borghini, M., Schroeder, K., & Sparnocchia, S. (2019). Investigation of internal wave mixing over the bottom topography of the deep Ionian sea. *Geophysical Research Abstracts*, *21*.
La Forgia, G., Adduce, C., & Falcini, F. (2018a). Laboratory investigation on internal solitary waves interacting with a uniform slope. *Advances in Water Resources*, *120*, 4–18. https://doi.org/10.1016/j.advwatres.2017.07.027
La Forgia, G., Adduce, C., Falcini, F., & Paola, C. (2019). Migrating bedforms generated by solitary waves. *Geophysical Research Letters*, *46*(9), 4738–4746. https://doi.org/10.1029/2019gl082511
la Forgia, G., Ottolenghi, L., Adduce, C., & Falcini, F. (2020a). Intrusions and solitons: Propagation and collision dynamics. *Physics of Fluids*, *32*(7), 076605. https://doi.org/10.1063/5.0011604
la Forgia, G., & Sciortino, G. (2019). The role of the free surface on interfacial solitary waves. *Physics of Fluids*, *31*(10), 106601. https://doi.org/10.1063/1.5120621
la Forgia, G., Tokyay, T., Adduce, C., & Constantinescu, G. (2018b). Numerical investigation of breaking internal solitary waves. *Physical Review Fluids*, *3*(10), 104801. https://doi.org/10.1103/physrevfluids.3.104801
la Forgia, G., Tokyay, T., Adduce, C., & Constantinescu, G. (2020b). Bed shear stress and sediment entrainment potential for breaking of internal solitary waves. *Advances in Water Resources*, *135*, 103475. https://doi.org/10.1016/j.advwatres.2019.103475
Lamb, K. G. (2002). A numerical investigation of solitary internal waves with trapped cores formed via shoaling. *Journal of Fluid Mechanics*, *451*, 109–144. https://doi.org/10.1017/s002211200100636x
Lamb, K. G. (2008). On the calculation of the available potential energy of an isolated perturbation in a density-stratified fluid. *Journal of Fluid Mechanics*, *597*, 415–427. https://doi.org/10.1017/s0022112007009743
Lamb, K. G. (2014). Internal wave breaking and dissipation mechanisms on the continental slope/shelf. *Annual Review of Fluid Mechanics*, *46*, 231–254. https://doi.org/10.1146/annurev-fluid-011212-140701
Ledwell, J., Montgomery, E., Polzin, K. L., St. Laurent, L. C., Schmitt, R. W., & Toole, J. M. (2000). Evidence for enhanced mixing over rough topography in the abyssal ocean. *Nature*, *403*(6766), 179–182. https://doi.org/10.1038/35003164
Long, R. R. (1953). Some aspects of the flow of stratified fluids: I. A theoretical investigation. *Tellus*, *5*(1), 42–58. https://doi.org/10.3402/tellusa.v5i1.8563
Lorenz, E. N. (1955). Available potential energy and the maintenance of the general circulation. *Tellus*, *7*(2), 157–167. https://doi.org/10.3402/tellusa.v7i2.8796
Lumley, R. V. (1964). The spectrum of nearly inertial turbulence in a stably stratified fluid. *Journal of Atmospheric Science*, *21*(1), 99–102. https://doi.org/10.1175/1520-0469(1964)021<0099:tsonit>2.0.co;2
Martorelli, E., Bosman, A., Casalbore, D., Chiocci, F. L., Conte, A. M., Di Bella, L., et al. (2020). Mid-to-late Holocene upper slope contourite deposits off Capo Vaticano (Mediterranean Sea): High-resolution record of contourite cyclicity, bottom current variability and sandy facies. *Marine Geology*, *431*, 106372.
Mashayek, A., Ferrari, R., Merrifield, S., Ledwell, J., St Laurent, L., & Naveira Garabato, A. (2017). Topographic enhancement of vertical turbulent mixing in the Southern Ocean. *Nature Communications*, *8*, 14197. https://doi.org/10.1038/ncomms14197
Massel, S. (2015). *Internal gravity waves in the shallow seas*. Springer.
McDougall, T. J., & Ferrari, R. (2017). Abyssal upwelling and downwelling driven by near-boundary mixing. *Journal of Physical Oceanography*, *47*(2), 261–283. https://doi.org/10.1175/jpo-d-16-0082.1
Michallet, H., & Ivey, G. (1999). Experiments on mixing due to internal solitary waves breaking on uniform slopes. *Journal of Geophysical Research: Oceans*, *104*(C6), 13467–13477. https://doi.org/10.1029/1999jc900037
Miyata, M. (1985). An internal solitary wave of large amplitude. *La mer*, *23*, 43–48.
Munk, W., & Wunsch, C. (1998). Abyssal recipes II: Energetics of tidal and wind mixing. *Deep Sea Research*, *45*(12), 1977–2010. https://doi.org/10.1016/s0967-0637(98)00070-3
Nash, J. D., & Moum, J. N. (2005). River plumes as a source of large-amplitude internal waves in the coastal ocean. *Nature*, *437*(5641), 400–403. https://doi.org/10.1038/nature03936
Nikurashin, M., & Ferrari, R. (2013). Overturning circulation driven by breaking internal waves in the deep ocean. *Geophysical Research Letters*, *40*(12), 3133–3137. https://doi.org/10.1002/grl.50542
Osborne, A., & Burch, T. (1980). Internal solitons in the Andaman Sea. *Science*, *208*(4443), 451–460. https://doi.org/10.1126/science.208.4443.451
Osborn, T. R. (1980). Estimates of the local rate of vertical diffusion from dissipation measurements. *Journal of Physical Oceanography*, *10*(1), 83–89. https://doi.org/10.1175/1520-0485(1980)010<0083:eotlro>2.0.co;2
Ottolenghi, L., Adduce, C., Inghilesi, R., Armenio, V., & Roman, F. (2016a). Entrainment and mixing in unsteady gravity currents. *Journal of Hydraulic Research*, *54*(5), 541–557. https://doi.org/10.1080/00221686.2016.1174961
Ottolenghi, L., Adduce, C., Inghilesi, R., Roman, F., & Armenio, V. (2016b). Mixing in lock-release gravity currents propagating up a slope. *Physics of Fluids*, *28*(5), 056604. https://doi.org/10.1063/1.4948760
Ottolenghi, L., Adduce, C., Roman, F., & la Forgia, G. (2020). Large eddy simulations of solitons colliding with intrusions. *Physics of Fluids*, *32*(9), 096606. https://doi.org/10.1063/5.0021196
Ozmidov, R. V. (1965). On the turbulent exchange in a stably stratified ocean. *Bulletin of the Academy of Sciences of the USSR*, *1*(8), 493–497.
Pan, J., Jay, D. A., & Orton, P. M. (2007). Analyses of internal solitary waves generated at the Columbia River plume front using SAR imagery. *Journal of Geophysical Research: Oceans*, *112*(C7). https://doi.org/10.1029/2006jc003688
Park, Y.-H., Lee, J.-H., Durand, L., & Hong, C.-S. (2014). Validation of Thorpe-scale-derived vertical diffusivities against microstructure measurements in the Kerguelen region. *Biogeosciences*, *11*(23), 6927–6937. https://doi.org/10.5194/bg-11-6927-2014
Patterson, M., Caulfield, C., McElwaine, J., & Dalziel, S. (2006). Time-dependent mixing in stratified Kelvin-Helmholtz billows: Experimental observations. *Geophysical Research Letters*, *33*(15). https://doi.org/10.1029/2006gl026949
Peltier, W., & Caulfield, C. (2003). Mixing efficiency in stratified shear flows. *Annual Review of Fluid Mechanics*, *35*(1), 135–167. https://doi.org/10.1146/annurev.fluid.35.101101.161144
Polzin, K. L., Toole, J. M., Ledwell, J. R., & Schmitt, R. W. (1997). Spatial variability of turbulent mixing in the abyssal ocean. *Science*, *276*(5309), 93–96. https://doi.org/10.1126/science.276.5309.93
Puig, P., Palanques, A., Guillén, J., & El Khatab, M. (2004). Role of internal waves in the generation of nepheloid layers on the northwestern Alboran slope: Implications for continental margin shaping. *Journal of Geophysical Research: Oceans*, *109*(C9). https://doi.org/10.1029/2004jc002394
Scotti, A., Beardsley, R., & Butman, B. (2006). On the interpretation of energy and energy fluxes of nonlinear internal waves: An example from Massachusetts Bay. *Journal of Fluid Mechanics*, *561*, 103–112. https://doi.org/10.1017/s0022112006000991
Shih, L. H., Koseff, J. R., Ivey, G. N., & Ferziger, J. H. (2005). Parameterization of turbulent fluxes and scales using homogeneous sheared stably stratified turbulence simulations. *Journal of Fluid Mechanics*, *525*, 193–214. https://doi.org/10.1017/s0022112004002587

Shroyer, E., Moum, J., & Nash, J. (2010). Energy transformations and dissipation of nonlinear internal waves over New Jersey's continental shelf. *Nonlinear Processes in Geophysics*, *17*(4), 345–360. https://doi.org/10.5194/npg-17-345-2010

Smyth, W., Moum, J., & Caldwell, D. (2001). The efficiency of mixing in turbulent patches: Inferences from direct simulations and microstructure observations. *Journal of Physical Oceanography*, *31*(8), 1969–1692. https://doi.org/10.1175/1520-0485(2001)031<1969:teomit>2.0.co;2

Stasna, M., & Lamb, K. G. (2002). Large fully nonlinear internal solitary waves: The effect of background current. *Physics of Fluids*, *14*(9), 2987–2999.

St. Laurent, L., Naveira Garabato, A. C., Ledwell, J. R., Thurnherr, A. M., Toole, J. M., & Watson, A. J. (2012). Turbulence and diapycnal mixing in Drake Passage. *Journal of Physical Oceanography*, *42*(12), 2143–2152. https://doi.org/10.1175/jpo-d-12-027.1

Sutherland, B., Barrett, K., & Ivey, G. (2013). Shoaling internal solitary waves. *Journal of Geophysical Research*. *118*(9), 4111–4124. https://doi.org/10.1002/jgrc.20291

Theiler, Q., & Franca, M. J. (2016). Contained density currents with high volume of release. *Sedimentology*, *63*(6), 1820–1842. https://doi.org/10.1111/sed.12295

Thorpe, S. A. (1974). Near-resonant forcing in a shallow two-layer fluid: A model for the internal surge in Loch Ness? *Journal of Fluid Mechanics*, *63*(3), 509–527. https://doi.org/10.1017/s0022112074001753

Thorpe, S. A. (1977). Turbulence and mixing in a Scottish Loch. *Philosophical Transactions of Royal Society A*, *286*(1334), 125–181. https://doi.org/10.1098/rsta.1977.0112

Thorpe, S. A. (2005). *The turbulent ocean*. Cambridge University Press.

Turkington, B., Eydeland, A., & Wang, S. (1991). A computational method for solitary internal waves in a continuously stratified fluid. *Studies in Applied Mathematics*, *85*(2), 93–127. https://doi.org/10.1002/sapm199185293

Venayagamoorthy, S. K., & Fringer, O. B. (2007). On the formation and propagation of nonlinear internal boluses across a shelf break. *Journal of Fluid Mechanics*, *577*, 137–159. https://doi.org/10.1017/s0022112007004624

Vlasenko, V., & Hutter, K. (2002). Numerical experiments on the breaking of solitary internal wavesover a slope–shelf topography. *Journal of Physical Oceanography*, *32*(6), 1779–1793. https://doi.org/10.1175/1520-0485(2002)032<1779:neotbo>2.0.co;2

Vlasenko, V., & Stashchuk, N. (2007). Nonlinear internal waves, internal bores, and turbulent mixing in the nearshore coastal environment. *Journal of Geophysical Research*, *112*, C11018. https://doi.org/10.1029/2007jc004107

Walter, R. K., Woodson, C. B., Arthur, R. S., Fringer, O. B., & Monismith, S. G. (2012). Nearshore internal bores and turbulent mixing in southern Monterey Bay. *Journal of Geophysical Research*, *117*(C7), C07017. https://doi.org/10.1029/2012jc008115

Winters, K., & D'Asaro, E. (1996). Diascalar flux and the rate of fluid mixing. *Journal of Fluid Mechanics*, *317*, 179–193. https://doi.org/10.1017/s0022112096000717

Winters, K., Lombard, P., Riley, J., & D'Asaro, E. (1995). Available potential energy and mixing in density-stratified fluids. *Journal of Fluid Mechanics*, *289*, 115–128. https://doi.org/10.1017/s002211209500125x

Woodson, C. (2018). The fate and impact of internal waves in nearshore ecosystems. *Annual Reviews of Marine Sciences*, *10*, 421–441. https://doi.org/10.1146/annurev-marine-121916-063619

Wuest, A., & Lorke, A. (2005). Validation of microstructure-based diffusivity estimates using tracers in lakes and oceans. In *Marine turbulence: Theories, observations and models*.

Wunsch, C., & Ferrari, R. (2004). Vertical mixing, energy, and the general circulation of the oceans. *Annual Reviews of Fluid Dynamics*, *36*, 281–314. https://doi.org/10.1146/annurev.fluid.36.050802.122121

Xu, C., & Stastna, M. (2019). Internal waves in a shear background current: Transition from solitary-wave regime to dispersive-wave regime. *Physical Review Fluids*, *4*(9), 094801. https://doi.org/10.1103/physrevfluids.4.094801